Mathematical Modelling of Engineering Problems
Vol. 12, No. 6, June, 2025, pp. 1849-1856
Journal homepage: http://iieta.org/journals/mmep

Cylindrical Conformal Antenna in a Homogeneous Plasma

Mohammad S. Al-Abadi[1*], Dhuha G. Hammood[1], Osman Shakirovich Dautov[2], Mohamed N. Shaaban[3]

[1] Department of Communications Engineering, University of Diyala, Baquba 32001, Iraq
[2] Department of Radio-Engineering and Telecommunications Systems, University of KNITU-KAI, Kazan 420111, Russia
[3] Electrical Engineering Department, Faculty of Engineering, Al-Azhar University, Qena 83523, Egypt

Corresponding Author Email: msmhhjk@yahoo.com

https://doi.org/10.18280/mmep.120603

Received: 16 March 2025
Revised: 8 May 2025
Accepted: 16 May 2025
Available online: 30 June 2025

Keywords:
conformal antenna, cylindrical slotted antenna, integro-functional equation method, Fourier-Bessel expansion, saddle-point method, plasma layer, radiation pattern, Drude model

ABSTRACT

Based on integro-functional equations method, an electrodynamic model of two-layer system with axial symmetry surrounding a cylindrical slotted antenna on a cylindrical aircraft is constructed to form a conformal antenna to the airframes shape. The study also demonstrates the radiation pattern calculations using Mathcad with respect to the frequency and influence of the curvature of the cylinder. In this paper, the application of the integro-functional equation method to model cylindrical conformal antennas in homogeneous plasma, which simplifies the analysis by avoiding internal plasma field calculations. The model is obtained in the form of expansions of fields in wave functions in orthogonal cylindrical coordinate systems. Electromagnetic waves emitted by the isolated slotted-cylindrical antenna pass through the plasma layer without losses if the applied angular frequency is equal to or greater than the plasma angular frequency. In addition, the radiation level is proportional to the radius of that antenna.

1. INTRODUCTION

The cylindrical slotted antenna was first proposed in 1938 by Alan D. Blumlein to use in television broadcasting with horizontal polarization and a circular radiation pattern in a horizontal plane [1]. One of the advantages of slot antennas is that they do not affect the aerodynamics of the objects on which they are established, which later determined their widespread use on aircraft, rockets, submarines, and other movable objects. In addition, slot antennas are widely used as ground antennas [2].

Several articles propose an approach that would make it possible to place an antenna on aircraft, drones or spacecraft without reducing its aerodynamic properties. In other word, to make the antenna more suitable in terms of form and purpose called conformal antenna. Or the antenna should be conformal to a prescribed shape. The shape can be some part of an airplane, high-speed train, or other vehicle. The purpose is to build the antenna so that it becomes integrated with the structure and does not cause extra drag [3]. The purpose can also be that the antenna integration makes the antenna less disturbing, less visible to the human eyes, for instance, in an urban environment. A typical additional requirement in modern defense systems is that the antenna not backscatter microwave radiation when illuminated by an enemy radar transmitter, i.e., it has stealth properties. Specifically, in this case it is better to use plasma as well [4, 5].

In addition, the properties of conformal antennas on a cylindrical surface which allow wide-angle scanning at the desired frequency and polarization for further use. Slot cylindrical antenna with an original device for matching with a feeder is proposed in the study [6]. Such that the original matching device ensures simple and convenient matching and tuning of an antenna with the operating frequency. The antenna is made as a longitudinal slot on a metal pipe with a diameter much smaller than the wavelength. At the same time the length of the slot is less than the wavelength in free space. In the study [7], a multilayered circular cylindrical conformal wide slot antenna show that the operating frequency depends on the size of the slot and to lesser degree to the radius of the cylinder. Such that the slot antenna is in the shape of a hexagon. Broadband characteristics antenna which can be used as communication and radar antenna presented as S band cylindrical waveguide slot omnidirectional antenna [8]. Antenna had an omnidirectional radiation characteristic in the E-plane and in H-plane had an 8-shape radiation characteristic approximately.

In addition to controlling the shape of the antenna according to the flying object, it is also necessary to test its operation in the presence of the plasma. Plasma, the fourth state of matter, has many applications in electromagnetic engineering [9-13]. It has played an important role in military applications. Plasma can transmit, reflect, and absorb the electromagnetic waves depending on the conditions of propagation of the electromagnetic waves. Therefore, there are many studies that investigate in effect of plasma on the work of antennas [14-17]. Reconfigurable slotted antenna using plasma tube in study [18], used to obtain a reconfigurable radiation pattern according to the state of plasma whether it was switched on or switched off. Such that when plasma is switched on, at 1 GHz, antenna have the possibility to radiate, but at 4 GHz, there is no radiation from the antenna. Therefore, when manufacturing

an antenna that is intended to work in plasma, it is imperative to take into consideration the difference between plasma frequency and antenna operating frequency. In study [19], a Faraday shield effect using plasma (fluorescent lamp) was presented to show the impact of the plasma on the gain of patch antenna put inside lamp. Plasma behaves like a transparent media or a Faraday shield effect, respectively at switching lamp ON or OFF. In addition, noticed that, at the operating frequency the parameters keep a good matching.

In conformal antenna, transmitters are placed on non-flat surfaces like spherical [20-22], cylindrical [23-25], conical [26, 27], and their combinations [28].

In general, the electrodynamic modeling of conformal antennas in plasma environments involves the application of several established numerical techniques, including the method of auxiliary sources (MAS), surface integral equations (SIE), and volume integral equations (VIE). Each of these methods exhibits unique strengths; however, they are confronted with significant challenges when dealing with complex, multi-layered antenna structures coated with plasma. The MAS, for instance, demonstrates proficiency in handling simple geometries but encounters difficulties in managing the intricacies of conformal antennas with plasma coatings. Conversely, VIE methods, while necessitating volumetric meshing across the entire frequency spectrum, incur substantial computational costs, particularly when high-resolution plasma layers are involved. SIE techniques, which dimensionally reduce the problem, often lead to the formation of large, dense system matrices that complicate computations and may potentially sacrifice precision.

This paper introduces a novel integro-functional equation method as an alternative to the conventional approaches mentioned above. This method offers several notable advantages. It allows for the modeling of external electromagnetic fields without the explicit consideration of the internal plasma field, thereby simplifying the system's complexity and reducing computational demands. The inherent scalar formulation of the method, stemming from the azimuthal symmetry of the magnetic field, contributes to an efficient analysis process. Furthermore, it excels in the treatment of boundary conditions and enables the utilization of Fourier-Bessel expansions for frequency-domain analysis. These characteristics render the proposed approach highly suitable for modeling conformal antennas with two dielectric and plasma layers. The method provides a robust and scalable solution that is superior to traditional numerical techniques in terms of computational efficiency and accuracy.

So, this investigation aims to develop a conformal antenna of cylindrical geometry, encircled by a dielectric material, with an overlying plasma layer. The study employs the ingenious approach of the integrable-functional equation methodology, which significantly streamlines the analytical process by circumventing the computation of internal plasma fields. Moreover, this research scrutinizes the feasibility of maintaining the antenna's optimal performance under such configurations.

2. PHYSICAL MODEL

When studying the influence of the plasma layer on the operation of on-board antennas, the main interest is in the field in the far zone (directional pattern) and the field near the radiating element, which determines the input impedance of the antenna, i.e., the field external to the plasma.

The geometry of this system that shown in Figure 1, represented with the following parameters:

R_o- The radius of the cylinder, where larger radius results in a higher radiation level due to the larger aperture area.

R_1- The first outer cylindrical radius represented by the thickness of the insulating layer surrounding the cylinder.

R_2- The second outer cylindrical radius represented by the thickness of the plasma layer that surrounds the dielectric layer.

ε_o, μ_o- dielectric parameters,

ε_i, μ_i- plasma parameters,

ε_e, μ_e- outer space parameters.

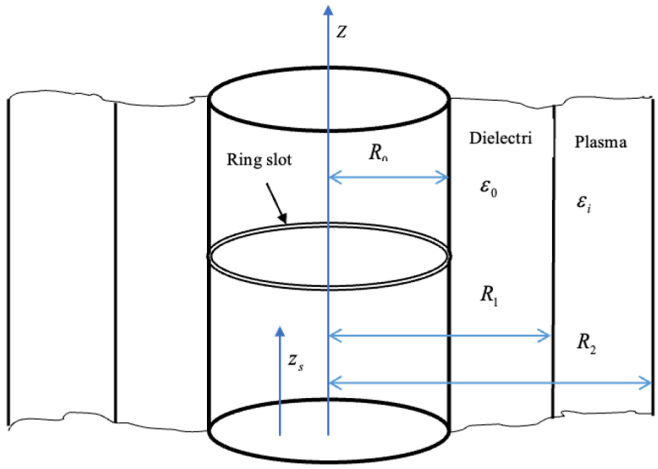

Figure 1. Slot antenna on a conductive cylinder under dielectric cover and plasma

3. MATHEMATICAL MODEL

The physical system under study is a cylindrical antenna with a slot embedded on a conductive surface, surrounded by two concentric cylindrical layers: an inner dielectric layer and an outer plasma layer as shown in Figure 1, where,

S- The surface of the body,

G_{i1}- Green's function of a homogeneous space with body parameters.

∇_s - Gradient operator with respect to coordinates of integration point.

$\bar{H}_e$- The desired external field consisting of an unperturbed field of external sources $\bar{H}_{oe}$, located in $V_{cme} \subset V_e$.

$\bar{H}_{oi}$- Unperturbed field of external sources located in V_i.

Using an integro-functional equation [29, 30], the total field beyond the plasma is given by:

$$L(l,H_e)=\pi\int_l \{H_e\frac{\partial(\rho_s G_{i1})}{\partial \nu} - \frac{\varepsilon_i}{\varepsilon_e}\frac{\partial(\rho_s H_e)}{\partial \nu}G_{i1}\}dl = \begin{cases} H_{oi} & (\vec{r}\in V_e) \\ -H_{pi} & (\vec{r}\in V_i) \end{cases} \quad (1)$$

This equation establishes a connection between the overall field and the source configuration across the body's surface by employing Green's function. The left-hand side of the equation can be separated into two distinct integral components, which correspond to the internal and external regions of the plasma layer.

$$L(l^{/},H_e)+L(l^{//},H_e)=\begin{cases}0 & (r\in V_e)\\ -H_{pi} & (r\in V_i)\end{cases} \tag{2}$$

To simplify the problem due to cylindrical symmetry, we expand the domains in terms of Fourier integrals (in the axial z direction) and Bessel functions (in the radial r direction) such that for $R_0 < r < R_1$:

$$H_e=\int_{-\infty}^{\infty}\left\{D(h)H_1^{(2)}(\nu_0 r)+A(h)J_1(\nu_0 r)\right\}e^{ihz}dh \tag{3}$$

where, $\nu_0=-i\sqrt{h^2-k_0^2}$, $D(h)$ and $A(h)$ are unknown spectral densities.

The integral operator on the inner surface becomes:

$$L(l^{/},H_e)=-\pi\int_{-\infty}^{\infty}\left\{H_e\frac{\partial(R_1G_{i1})}{\partial R_1}-\frac{\varepsilon_i}{\varepsilon_0}\frac{\partial(R_1H_e)}{\partial R_1}G_{i1}\right\}dz_{l^{/}} \tag{4}$$

where, the Green's function G_{i1} is expanded for cylindrical geometry (first azimuthal harmonic n=1), identical with Eq. (5),

$$G_{i1}=-\frac{ik_i}{2\pi}\sum_{n=1}^{\infty}\frac{2n+1}{n(n+1)}\psi_n(k_i r^{/})\xi_n^{(2)}(k_i r)P_n^1(\cos\theta^{/})P_n^1(\cos\theta) \tag{5}$$

and can be obtained from the well-known representation of the Green's function in cylindrical coordinates (1) and written as:

$$G_{i1}=\frac{1}{4\pi i}\int_{-\infty}^{\infty}\begin{cases}H_1^{(2)}(\nu_i r)J_1(\nu_i r^{/}) & (r^{/}<r)\\ J_1(\nu_i r)H_1^{(2)}(\nu_i r^{/}) & (r^{/}>r)\end{cases}e^{ih(z-z^{/})}dh \tag{6}$$

where, $\nu_i=-i\sqrt{h^2-k_i^2}$.

Assuming linearity, i.e., $r^{/}=R_1$ and $z^{/}=z_{l^{/}}$.

Substituting (3) and (6) into (4), the integral operator becomes:

$$L(l^{/},H_e)=\frac{\pi i}{2}\int_{-\infty}^{\infty}\begin{cases}(D(h)d_h+A(h)a_h)J_1(\nu_i r) & (r<R_1)\\ (D(h)d_j+A(h)a_j)H_1^{(2)}(\nu_i r) & (r>R_1)\end{cases}e^{ihz}dh \tag{7}$$

where,

$$d_h=H_1^{(2)}(\nu_0R_1)\frac{\partial(R_1H_1^{(2)}(\nu_iR_1))}{\partial R_1}-\frac{\varepsilon_i}{\varepsilon_0}\frac{\partial(R_1H_1^{(2)}(\nu_0R_1))}{\partial R_1}H_1^{(2)}(\nu_iR_1), \tag{8}$$

$$a_h=J_1(\nu_0R_1)\frac{\partial(R_1H_1^{(2)}(\nu_iR_1))}{\partial R_1}-\frac{\varepsilon_i}{\varepsilon_0}\frac{\partial(R_1J_1(\nu_0R_1))}{\partial R_1}H_1^{(2)}(\nu_iR_1), \tag{9}$$

$$d_J=H_1^{(2)}(\nu_0R_1)\frac{\partial(R_1J_1(\nu_iR_1))}{\partial R_1}-\frac{\varepsilon_i}{\varepsilon_0}\frac{\partial(R_1H_1^{(2)}(\nu_0R_1))}{\partial R_1}J_1(\nu_iR_1), \tag{10}$$

$$a_J=J_1(\nu_0R_1)\frac{\partial(R_1J_1(\nu_iR_1))}{\partial R_1}-\frac{\varepsilon_i}{\varepsilon_0}\frac{\partial(R_1J_1(\nu_0R_1))}{\partial R_1}J_1(\nu_iR_1). \tag{11}$$

Field in the outer space ($R_2 < r < \infty$) has the following integral representation:

$$H_e=\int_{-\infty}^{\infty}B(h)H_1^{(2)}(\nu_e r)e^{ihz}dh\ (\nu_e=-i\sqrt{h^2-k_e^2}) \tag{12}$$

and for the integral operator with respect to the outer surface of the plasma layer in (2), we obtain:

$$L(l^{//},H_e)=-\frac{\pi i}{2}\int_{-\infty}^{\infty}\begin{cases}B(h)b_hJ_1(\nu_i r)\\ B(h)b_jH_1^{(2)}(\nu_i r)\end{cases}e^{ihz}dh \quad (r<R_2);(r>R_2) \tag{13}$$

where:

$$b_h=H_1^{(2)}(\nu_eR_2)\frac{\partial(R_2H_1^{(2)}(\nu_iR_2))}{\partial R_2}-\frac{\varepsilon_i}{\varepsilon_e}\frac{\partial(R_2H_1^{(2)}(\nu_eR_2))}{\partial R_2}H_1^{(2)}(\nu_iR_2) \tag{14}$$

$$b_J=H_1^{(2)}(\nu_eR_2)\frac{\partial(R_2J_1(\nu_iR_2))}{\partial R_2}-\frac{\varepsilon_i}{\varepsilon_e}\frac{\partial(R_2H_1^{(2)}(\nu_eR_2))}{\partial R_2}J_1(\nu_iR_2). \tag{15}$$

These integrals take advantage of well-known properties and derivatives of Bessel functions, such as recurrence relations and asymptotic forms.

Using the known functional relation for Bessel functions of any kind:

$$\frac{\partial(zZ_1(z))}{\partial z}=zZ_0(z)$$

In the relations Eqs. (8)-(10), (11), (14), (15), the derivatives can be replaced by the Bessel functions themselves.

$$\frac{\partial(R_1H_1^{(2)}(\nu_iR_1))}{\partial R_1}=\nu_iR_1H_0^{(2)}(\nu_iR_1).$$

The boundary conditions in the plasma layer are expressed by the integral Green's function (IGF) equations, which are divided into two radial regions as shown in Eq. (16). The IGF formulation applied to a layered cylindrical structure can be written as:

$$L(l^{/}, H_e) + L(l^{//}, H_e) = 0$$
$$(R_0 < r < R_1); (R_2 < r < \infty) \quad (16)$$

The two constituents of Eq. (16) represent integral operators that are applied to the magnetic field components situated within the dielectric and plasma layers. It is essential to note that the total magnetic field, or its Green's function representation, is subject to the rigorous adherence of physical boundary conditions at the interfaces between these regions. These boundary conditions typically necessitate the continuity of both the tangential electric and magnetic fields across the dielectric-plasma boundaries. In addition, this equation, considering the representations Eqs. (7), (13), leads to a system of equations for the spectral densities. For the first condition in Eq. (16), we obtain:

$$D(h)d_h + A(h)a_h - B(h)b_h = 0 \quad (17)$$

and for the second, respectively:

$$D(h)d_J + A(h)a_J - B(h)b_J = 0 \quad (18)$$

D(h), A(h), B(h) are spectral response functions or integral kernels, depending on the geometry and material parameters.

It is convenient to solve this linear system with respect to A(h) and B(h) assuming a temporarily known spectral density D(h):

$$A(h) = \sigma D(h) \quad (19)$$

$$B(h) = \gamma D(h) \quad (20)$$

For the coefficients σ and γ we have the system of equations:

$$\sigma a_h - \gamma b_h = -d_h$$
$$\sigma a_J - \gamma b_J = -d_J \quad (21)$$

The solution of which has the form:

$$\sigma = \frac{d_J b_h - d_h b_J}{a_h b_J - a_J b_h} \quad (22)$$

$$\gamma = \frac{d_J a_h - d_h a_J}{a_h b_J - a_J b_h} \quad (23)$$

Using the boundary condition of the electric field tangent to the surface (voltage-excited slot). Unknown spectral density $D(h)$ can be found from the boundary conditions on the surface of the cylinder. The tangential component of the electric field E_{ez} can be determined from the magnetic field:

$$E_{ez} = -\frac{i}{\omega\varepsilon_e}\frac{1}{r}\frac{\partial(rH_e)}{\partial r} \quad (24)$$

Using representation (12) and formulas for the derivatives of Bessel functions, we obtain the following representation for the tangential component of the electric field on the cylinder surface:

$$E_{ez}\big|_{r=R_0} = -\frac{i}{\omega\varepsilon_e}\int_{-\infty}^{\infty} \nu_0 D(h)\left\{H_0^{(2)}(\nu_0 R_0) + \sigma(h) J_0(\nu_0 R_0)\right\} e^{ihz} dh \quad (25)$$

On the other hand, for slot on a conductive cylinder with an applied voltage U_s and coordinate Z_s (slot):

$$E_{ez} = U_s \delta(z - z_s) = \frac{U_s}{2\pi}\int_{-\infty}^{\infty} e^{ih(z-z_s)} dh \quad (26)$$

where, for the spectral density for Fourier transform of the slot voltage profile $D(h)$:

$$D(h) = \frac{iU_s \omega\varepsilon_e e^{-ihz_s}}{2\pi\nu_0[H_0^{(2)}(\nu_0 R_0) + \sigma(h) J_0(\nu_0 R_0)]}. \quad (27)$$

To find the radiation pattern (far field), we can use directly the integral representation Eq. (12) to estimate the value of the integral by the saddle-point method. The electric field in the far field has a component of E_θ, where, $E_\theta = W_e H_e$ and $w_e = \sqrt{\frac{\mu_e}{\varepsilon_e}}$ - wave resistance of the medium in the external space. In the far zone, it can be represented in the form:

$$E_\theta = G_e(r) F_\theta(\theta) \quad (28)$$

where, $G_e = \frac{e^{-ik_e r}}{4\pi r}$.

The resulting radiation pattern is:

$$F_\theta(\theta) = 4W_e \gamma(h) D(h)\big|_{h=-k_e\cos\theta} \quad (29)$$

This model efficiently captures the complex interaction of the cylindrical antenna with the surrounding dielectric layers and neighboring plasma, resulting in radiation properties that are significantly influenced by the particular plasma conditions and the antenna's design across a broad spectrum of frequencies.

4. RESULTS AND DISCUSSION

When constructing the models, one of the features of the method of integro-functional equations is realized, consisting in the possibility of using the equation relative to the external field, without including the field inside the plasma in the number of unknowns. In this case, the dimension of the algebraic system is half as small as in the method of stitching fields.

To investigate the frequency dependence of the radiation pattern for this antenna, assuming that, R_O =1 m, $R_1 = R_O$ +0.05 m, $R_2 = R_1$ +0.08 m and consider the following parameters of the system:

- The range of operating frequency is 1 GHz to 100 GHz,
- The plasma electron density (n_e) is 10^{10} cm^{-3},
- Plasma collision frequency (ν) is 10^{11},
- The relative permittivity of dielectric material (ε_r) of the first layer is 5,
- Loss tangent of the dielectric material (tgδ) is 0.005,
- Applying several different values of operating frequency like 1 GHz, 2.3 GHz, 4.8 GHz, 10 GHz, 75 GHz, and 100 GHz as shown in Figures 2-10.

In this research endeavor, the Drude model and Maxwell's equations were employed to derive dispersion relations pertaining to plasma wave propagation. Utilizing Mathcad as

the computational tool, these intricate equations, which are dependent on factors such as electron charge, collision frequency, and background density, were solved numerically. The software's inherent capabilities for handling complex arithmetic greatly simplified the process of computing expressions within the frequency domain. Consequently, Mathcad's built-in numerical solvers, namely the root function and the find function, were instrumental in obtaining the solutions. The visual representation of the outcomes was achieved through the creation of graphical outputs, which served to illustrate critical properties of the plasma, encompassing scattering behavior and damping effects with clarity by applying several different values of operating frequency like 1 GHz, 2.3 GHz, 4.8 GHz, 10 GHz, 75 GHz, and 100 GHz are shown in Figures 2-8.

Since the Drude model serves as the fundamental framework elucidating the interaction between electromagnetic waves and the plasma sheath enveloping a cylindrically-configured conformal antenna, it is crucial to comprehend that this paradigm considers plasma as a collection of non-bound electron species. Within this theoretical construct, the electrons are influenced by oscillatory electric fields emanating from incoming electromagnetic waves and may undergo attenuation following collisions with neutral particles. This dampening effect is contingent upon the specific frequency of the interacting electromagnetic radiation.

According to Drude model, the angular frequency of antenna is $\omega = 2\pi f$ and the angular frequency of plasma [18] is:

$$\omega_p = \sqrt{\frac{n_e\, e^2}{m_e\, \varepsilon_o}} \tag{30}$$

where, n_e is an electron density of plasma cm^{-3}, which is directly determines the plasma frequency ω_p, e is the charge of electron (1.6×10^{-19}) coulombs, m_e is the mass of electron (0.91×10^{-30}) kg, and ε_o is the relative permittivity of vacuum.

The relative permittivity of the plasma, which governs how electromagnetic waves propagate, is given by the Drude formula:

$$\varepsilon_r = 1 - \frac{{\omega_p}^2}{\omega(\omega - jv)} \tag{31}$$

where, ε_r is the complex plasma permittivity, and v is the electron-neutral collision frequency. A high rate of collisions within the plasma medium leads to an enhanced attenuation of energy in the form of thermalization, particularly when the angular frequency of the electromagnetic waves, ω, approaches the plasma frequency, ω_p. This phenomenon is detrimental to the overall radiation efficiency. Conversely, a reduced frequency of interparticle collisions is conducive to a more optically transparent plasma state, facilitating superior propagation characteristics for electromagnetic waves, notably at elevated frequencies.

So, the properties of the electromagnetic waves radiated from the antenna (whether they are absorbed, reflected or passing through the plasma layer) depend on the threshold or the relationship between the angular operating frequency (ω) and the plasma frequency (ω_p) [31]. Such that, at $\omega \geq \omega_p$, the electromagnetic waves passing through plasma layer almost without loss. The plasma permittivity becomes positive and electromagnetic waves can propagate through the plasma layer with minimal attenuation. In this case, the plasma behaves like a lossless dielectric. This condition enables effective radiation from the antenna through the plasma layer.

Conversely, when $\omega < \omega_p$, the real part of plasma permittivity becomes negative, and plasma behaves like a reflective or absorbate medium. EM waves are reflected or absorbed or both situations causing a decrease in antenna gain.

Applying that taken values of antenna operation frequency and plasma frequency using Mathcad, the angular operating frequency (ω) is almost equal to the angular plasma frequency (ω_p) and upwards.

Using the saddle-point approximation technique, we derive the analytical expression for the beam pattern of a slot antenna upon a cylindrical substrate, as depicted in the accompanying figures. The normalization of the presented diagram is performed in a manner that, upon multiplication of its numerical values with the scalar Green's function, yields the magnitude of the electric field at any specified point at a particular distance from the cylinder.

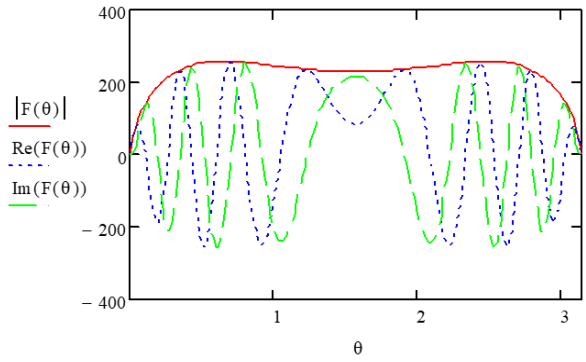

Figure 2. Radiation pattern at the frequency 1 GHz

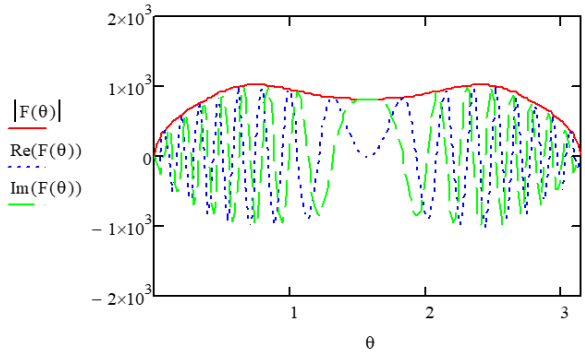

Figure 3. Radiation pattern at the frequency 2.3 GHz

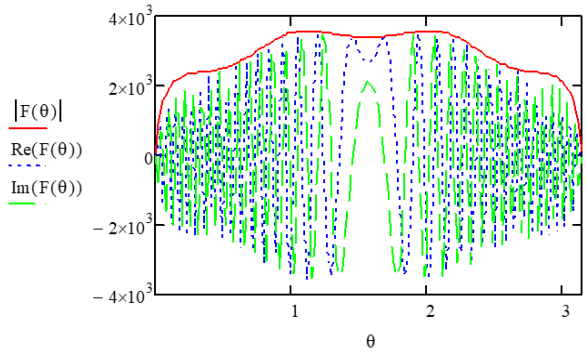

Figure 4. Radiation pattern at the frequency 4.8 GHz

This allows us to investigate both the change in the shape of the radiation pattern and the radiation level.

The figures show that, the electromagnetic waves passing through plasma layer without losses as a result of achieving the relationship ($\omega \geq \omega_p$).

In general, whether the antenna type used is spherical slotted [22] or cylindrical slotted, at a plasma electron density of 10^{10} cm^{-3}, a large level of radiation is observed when the condition of equality or increase in the angular frequency of the plasma angular frequency ($\omega \geq \omega_p$) is met. As a comparison between the two types, it can be noticed that the difference is in the shape of the radiation pattern and the beamwidth. The cylindrical antennas exhibit an intrinsic characteristic of generating a more extensive radiation pattern, primarily attributable to their geometric configuration. In contrast, spherical antennas demonstrate a higher degree of efficiency in concentrating electromagnetic energy, thereby yielding narrower beamwidths and enhanced directivity. So, we see that the radiation pattern in the spherical antenna is more directional with lower magnitude (Figure 5) compared to the cylindrical antenna (Figure 2), which has a wide beamwidth.

In addition, with a plasma density of 10^{10} cm^{-3}, the dielectric permittivity of the dielectric coating and the plasma are positive. Therefore, the main important parameter is the thickness of the first layer, which determines the modulation resonance. Therefore, the calculated peaks are clearly determined for a certain thickness of the dielectric coating itself. The plasma layer can support the propagation of modulations, and the energy penetration in the outer region is almost maintained at its constant thickness.

In addition, we notice that as the operating frequency of the antenna increases relative to the plasma frequency, level of radiation pattern increases more and more as it is extremely clear in the Figures 7 and 8.

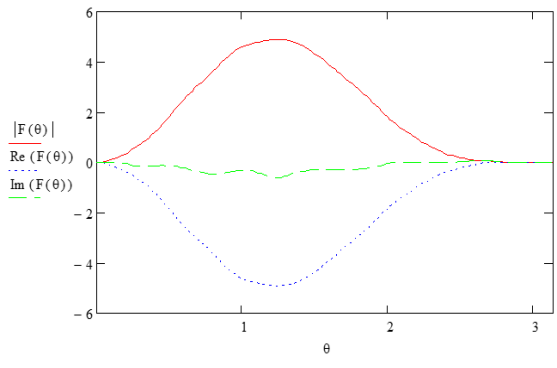

Figure 5. Radiation pattern for spherical slotted antenna at frequency 1 GHz

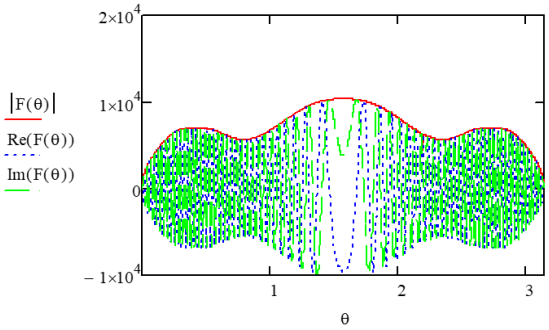

Figure 6. Radiation pattern at the frequency 10 GHz

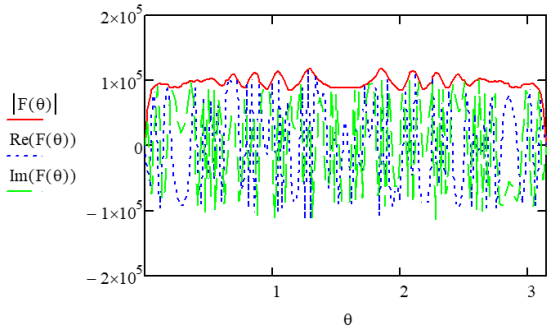

Figure 7. Radiation pattern at the frequency 75 GHz

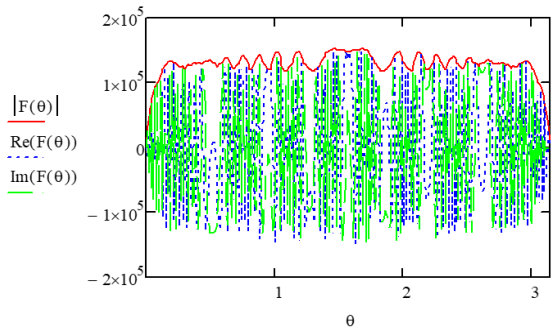

Figure 8. Radiation pattern at the frequency 100 GHz

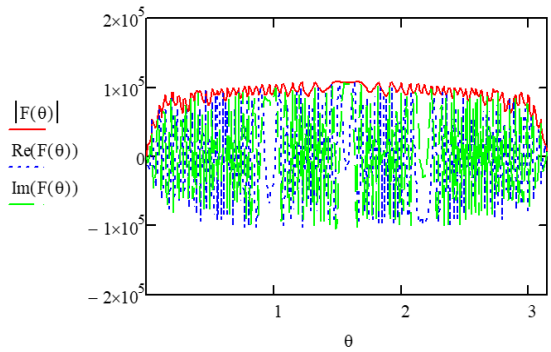

Figure 9. Radiation pattern at the frequency 100 GHz and R_o=0.5 m

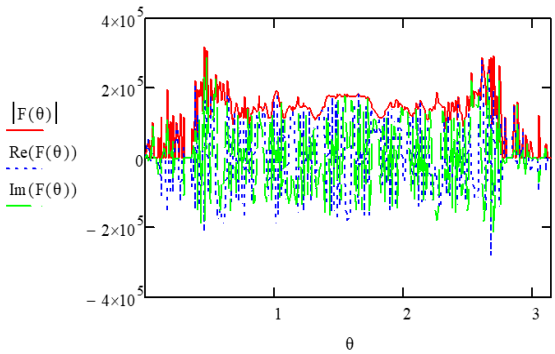

Figure 10. Radiation pattern at the frequency 100 GHz and R_o=1.4 m

It is also noticed from the figures, that there are differences in the shape of the radiation pattern and appearance of some harmonics resulting from the difference between the fundamental frequency of the antenna design and the other used frequencies.

By incorporating the Drude model with the integro-

functional equation approach, the study's analysis effectively foretells radiation pattern variations over diverse frequency bands. The depicted radiation patterns in Figures 2 through 10 illustrate a significant alteration in behavior beyond the operational frequency ω, thus substantiating the Drude model's predictions concerning dispersion.

This frequency-dependent characteristic is of paramount importance in the design of antennas intended for the aerospace and defense sectors, where plasma layers might occur naturally due to rapid movement through the atmosphere, such as with reentry vehicles and aircraft traveling at supersonic speeds or be deliberately produced for the enhancement of stealth capabilities or tuning purposes.

To check the conformability of the antenna to the aircraft surface curvature, the effect of the radius cylindrical antenna must be studied. The degree of influence of the aircraft surface curvature depends on the orientation of the slot antenna relative to the surface. For a fixed voltage across the slot, the radiation level is proportional to the radius. The shape of the radiation pattern can vary significantly. This is confirmed by the calculations for 100 GHz shown in Figures 9 and 10. A similar regularity is observed at other frequencies.

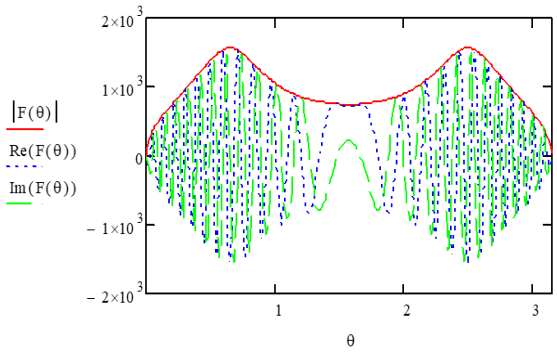

Figure 11. Radiation pattern at the frequency 2.3 GHz and R_o=1.5 m

Figure 11 shows the radiation pattern at 2.3 GHz at R_o=1.5 m. The nature of the changes in the shape and the level of the radiation pattern is seen from a comparison with the radiation pattern at R_o=1 m at the same frequency, shown in Figure 3. Where is there is an increase in the radiation pattern level at an antenna with a radius of 1.5 meters.

5. CONCLUSION

This study presents an efficient electrodynamic model employing the integra-functional equation method for evaluating cylindrical slotted antennas with dielectric and plasma coverings. Unlike conventional techniques, such as auxiliary sources, surface integral equations, and volume integral equations, it provides accurate external field computations without explicit internal plasma modeling, reducing computational complexity, especially in axial symmetry. The Drude model's incorporation reveals the antenna's radiation characteristics are significantly influenced by the relationship between the operating frequency and the plasma frequency. The radiation efficiency is maximized when the frequency is equal to or exceeds the plasma frequency, as this minimizes wave attenuation. Conversely, lower frequencies cause wave reflection and absorption, degrading performance. The research confirms that antenna curvature, determined by the cylinder radius, impacts radiation intensity and pattern, with larger radii leading to increased radiation levels due to a larger effective aperture. This insight is crucial for enhancing antenna designs in aerospace and defense, particularly for conformal antennas operating in plasma-rich environments. The model represents a substantial advancement for modern communication systems and stealth technologies which are contingent upon the effective functioning of such antennas.

REFERENCES

[1] British Patent No. 515684. Improvements in or relating to high frequency electrical conductors or radiators. https://www.aktuellum.com/content/images/2024/03/patents/515684.pdf.

[2] Voytovich N.I., Klygach D.S., Repin, N.N. (2013). Slot Turnstile Antenna. In 7th European Conference on Antennas and Propagation (EuCAP-2013), Gothenburg, Sweden, pp. 1208-1212. https://ieeexplore.ieee.org/document/6546471/.

[3] Josefsson, L., Persson, P. (2006). Conformal Array Antenna Theory and Design. John Wiley & Sons.

[4] Dautov, O.S., Al-Abadi, M.S., Al-Anbagi, H.N. (2020). New proposed spherical slotted antenna covered by the layers of dielectric material and plasma. International Journal of Electrical and Computer Engineering, 10(2): 1728-1735. http://doi.org/10.11591/ijece.v10i2.pp1728-1735

[5] Dautov, O.S., Al-Abadi, M.S. (2021). The optimal excitation voltage for spherical slotted antenna coated by two layers of dielectric material and plasma. In 2021 International Siberian Conference on Control and Communications (SIBCON), Kazan, Russia, pp. 1-6. https://doi.org/10.1109/SIBCON50419.2021.9438871

[6] Denis Klygach, V.A. Dumchev, N.N. Repin, N.V. (2015). Цилиндрическая щелевая антенна. Компьютерные технологии, Управление, Радиоэлектроника, 15(2): 21-31. https://doi.org/10.14529/ctcr150203

[7] Monajati, A.R., Hassani, H.R., Moghadasi, M.N. (2008). Wideband multi-layered cylindrical conformal slot antenna. IEICE Electronics Express, 5(17): 631-637. https://doi.org/10.1587/elex.5.631

[8] Fang, Z. (2018). Design of S band cylindrical waveguide slot omnidirectional antenna. In SPACOMM 2018: The Tenth International Conference on Advances in Satellite and Space Communications, Athens, Greece, pp. 48-50.

[9] Dewitt, B.T., Burnside, W.D. (1988). Electromagnetic scattering by pyramidal and wedge absorber. IEEE Transactions on Antennas and Propagation, 36(7): 971-984. https://doi.org/10.1109/8.7202

[10] Salisbury, W.W. (1952). U.S. Patent No. 2,599,944. Washington, DC: U.S. Patent and Trademark Office.

[11] Engheta, N. (2002). Thin absorbing screens using metamaterial surfaces. In IEEE Antennas and Propagation Society International Symposium (IEEE Cat. No. 02CH37313), San Antonio, TX, USA, pp. 392-395. https://doi.org/10.1109/APS.2002.1016106

[12] Kaur, M., Khanna, R., Sharma, A. (2019). Radar cross section reduction techniques using metamaterials. International Journal of Innovative Technology and Exploring Engineering, 8(9s): 103-111.

https://doi.org/10.35940/ijitee.I1016.0789S19
[13] Laroussi, M. (1995). Interaction of microwaves with atmospheric pressure plasmas. International Journal of Infrared and Millimeter Waves, 16(12): 2069-2083. https://doi.org/10.1007/BF02073410
[14] Smith, T., Golden, K. (1965). Radiation patterns from a slotted cylinder surrounded by a plasma sheath. IEEE Transactions on Antennas and Propagation, 13(5): 775-780. https://doi.org/10.1109/TAP.1965.1138536
[15] Burman, R. (1966). Electromagnetic radiation from a slotted-cylinder antenna with an inhomogeneous sheath. Electronics Letters, 2(3): 102-103. https://doi.org/10.1049/el:19660083
[16] Marini, J.W. (1961). Radiation and admittance of a slotted-sphere antenna surrounded by a plasma sheath. Planetary and Space Science, 6: 116-122. https://doi.org/10.1016/0032-0633(61)90011-3
[17] Nandhitha, N.M. (2018). Design of linear plasma position controllers with intelligent feedback systems for Aditya tokamak. International Journal of Electrical & Computer Engineering, 8(5): 2904-2909. https://doi.org/10.11591/ijece.v8i5.pp2904-2909
[18] Barro, O.A., Himdi, M., Vettikalladi, H. (2019). Reconfigurable slotted cylindrical waveguide and coaxial array antenna using plasma. In 2019 13th European Conference on Antennas and Propagation (EuCAP), Krakow, Poland, pp. 1-4.
[19] Barro, O.A., Himdi, M., Lafond, O. (2015). Reconfigurable patch antenna radiations using plasma faraday shield effect. IEEE Antennas and Wireless Propagation Letters, 15: 726-729. https://doi.org/10.1109/LAWP.2015.2470525
[20] Braaten, B.D., Roy, S., Irfanullah, I., Nariyal, S., Anagnostou, D.E. (2014). Phase-compensated conformal antennas for changing spherical surfaces. IEEE Transactions on Antennas and Propagation, 62(4): 1880-1887. https://doi.org/10.1109/TAP.2014.2298881
[21] Knott, P. (2007). Design and experimental results of a spherical antenna array for a conformal array demonstrator. In 2007 2nd International ITG Conference on Antennas, Munich, Germany, pp. 120-123. https://doi.org/10.1109/INICA.2007.4353945
[22] Dautov, O.S., Al-Abadi, M.S., Ahmed, R.K. (2019). Radiation pattern of spherical slotted antenna coated by dielectric material and plasma. In 2019 International Conference on Advanced Science and Engineering (ICOASE), Zakho - Duhok, Iraq, pp. 165-169. https://doi.org/10.1109/ICOASE.2019.8723689
[23] Qin, J.J., Yin, Z.W., Cao, X.Y. (2006). MOM analysis of cylindrical conformal dipole array. In 2006 7th International Symposium on Antennas, Propagation & EM Theory, Guilin, China, pp. 1-4. https://doi.org/10.1109/ISAPE.2006.353394
[24] Nadar, K.P., Jeyaprakasam, V., Mariapushpam, I.T., Vivekanand, C.V., Eswaralingam, A.D., Louis, M.T., Arul Raj, J.X., Jibril, H.A., Chellappa, A.S., Muthukutty, R.K., Gopalakrishnan, S. (2023). Design and analysis of microstrip patch antenna array and electronic beam steering linear phased antenna array with high directivity for space applications. ACS Omega, 8(45): 43197-43217. https://doi.org/10.1021/acsomega.3c06691
[25] Yinusa, K.A. (2018). A dual-band conformal antenna for GNSS applications in small cylindrical structures. IEEE Antennas and Wireless Propagation Letters, 17(6): 1056-1059. https://doi.org/10.1109/LAWP.2018.2830969
[26] Xu, K., Ye, D., Zhu, Z., Huangfu, J., Sun, Y., Li, C., Ran, L. (2014). Analytical beam forming for circularly symmetric conformal apertures. IEEE Transactions on Antennas and Propagation, 63(4): 1458-1464. https://doi.org/10.1109/TAP.2014.2382663
[27] Xu, H., Cui, J., Duan, J., Zhang, B., Tian, Y. (2019). Versatile conical conformal array antenna based on implementation of independent and endfire radiation for UAV applications. IEEE Access, 7: 31207-31217. https://doi.org/10.1109/ACCESS.2019.2903198
[28] Gao, Y., Wu, Q. (2024). Analysis of cylindrically conformal dipole array using periodic stratified media green's function. In 2024 IEEE International Conference on Computational Electromagnetics (ICCEM), Nanjing, China, pp. 1-3. https://doi.org/10.1109/ICCEM60619.2024.10559134
[29] Markov, G.T., Chaplin, A.F. (1983). The Excitation of Electromagnetic Waves. Moscow Izdatel Radio Sviaz.
[30] Dautov, O.S. (1991). Equivalence of integral and integrofunctional equations in electrodynamic problems of diffraction by inhomogeneous bodies. Radiophysics and Quantum Electronics, 34(8): 749-756. https://doi.org/10.1007/BF01036982
[31] Lavrushev, V.N., Dautov, O.S., Al-Abadi, M.S., Almakki, A.N.J. (2023). Scattering of electromagnetic waves by plasma layer sandwiched between two layers of thin glass. Przeglad Elektrotechniczny, 99(4): 102-106. https://doi.org/10.15199/48.2023.04.18

NOMENCLATURE

R_o	radius of the cylinder, m
R_1	radius of the first layer, m
R_2	radius of the second layer, m
S	surface of the body
$F_\theta(\theta)$	The level of the adiation pattern

Greek symbols

ω	angular frequency of antenna, rad/sec
ω_p	angular frequency of plasma, rad/sec
G_{i1}	Green's function of a homogeneous space with body parameters
∇_s	Gradient operator with respect to coordinates of integration point
$\bar{H}_e$	the desired external field
$\bar{H}_{oi}$	The unperturbed field of external sources